Finite element modelling of magnetotelluric fields in 2-D structures with arbitrary anisotropy

Yuguo Li
Institut für Geophysik, Universität Göttingen

We consider 2-D models with anisotropic sections using the finite element (FE) technique. **Part 1** gives the boundary value problem, **Part 2** describes the numerical realization of the FE algorithm, **Part 3** compares results from the FE algorithm with the finite difference solution of Pek & Verner (1997). **Part 4** presents modelling results for various types of anisotropy: horizontal, vertical and dipping anisotropy.

1 The boundary value problem

The two basic second-order differential equations for the field components E_x and H_x in strike direction (Fig. 1) are

$$\frac{1}{i\omega\mu_0}\nabla^2 E_x + CE_x + A\frac{\partial H_x}{\partial y} - B\frac{\partial H_x}{\partial z} = 0, \tag{1}$$

$$\nabla\cdot(\underline{\underline{\tau}}\nabla H_x) + i\omega\mu_0 H_x - \frac{\partial(AE_x)}{\partial y} + \frac{\partial(BE_x)}{\partial z} = 0, \tag{2}$$

where

$$D = \sigma_{yy}\sigma_{zz} - \sigma_{yz}\sigma_{zy}, \qquad A = (\sigma_{yx}\sigma_{zy} - \sigma_{zx}\sigma_{yy})/D,$$
$$B = (\sigma_{zx}\sigma_{yz} - \sigma_{yx}\sigma_{zz})/D, \qquad C = \sigma_{xx} + \sigma_{xy}B + \sigma_{xz}A,$$

$$\underline{\underline{\tau}} = \frac{1}{D}\begin{pmatrix} \sigma_{yy} & \sigma_{yz} \\ \sigma_{zy} & \sigma_{zz} \end{pmatrix}.$$

Because of the anisotropy, the equations for E_x and H_x are coupled through the first-order partial derivatives. Consequently, there are no separate TE and TM-modes in the general anisotropic case. Hence, equations (1) and (2) must be solved jointly towards E_x **and** H_x.

The boundary conditions for electric and magnetic fields are as follows: On the outer boundary of the model, Dirichlet boundary conditions are set, constructed from 1-D solutions for the corresponding layered Earth at the left and right hand side of the model. On inner boundaries (layer boundaries and section boundaries), the tangential components of both electric and magnetic fields, E_t and H_t, must be continuous.

2 The finite element method

The numerical evaluation of the problem, posed by eqs. (1) and (2), is based on the finite element approach. The approximation is performed on a model area Ω that entirely embraces the zone of the 2-D inhomogeneities, and extends far enough in all directions for the anomalous fields to fade out to sufficient smallness on the external boundary of Ω. To avoid the singularity of (2) due to vanishing conductivity within the insulating air layer above the earth, we assume that the air has a very small, but non-zero conductivity.

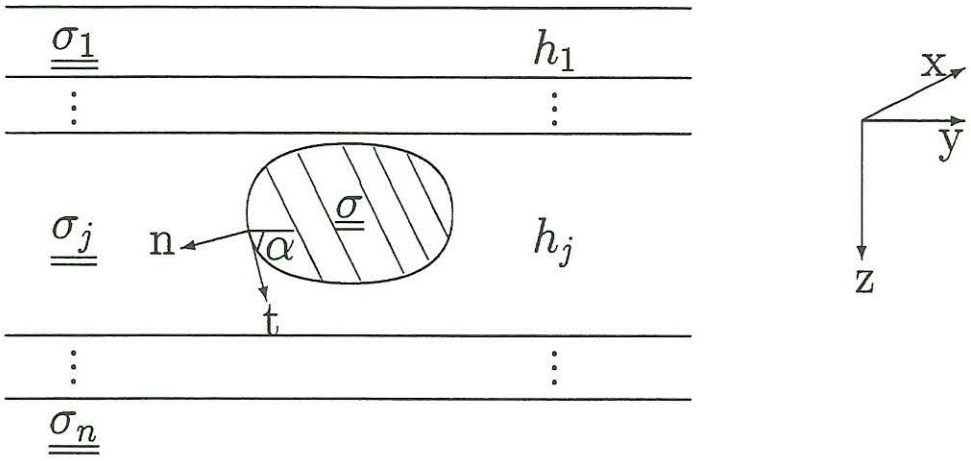

Fig. 1 2D anisotropic inhomogeneity in an N layered earth, which can be in general anisotropic and different for either hand side of the model.

The method of weighted residuals is used to derive the integral equations from the differential equations (1) and (2). Eq. (1) is multiplied by an arbitrary variation of the electric field δE_x and integrated over the model area Ω:

$$\int_\Omega \left(\frac{1}{i\omega\mu_0} \nabla^2 E_x + C E_x + A \frac{\partial H_x}{\partial y} - B \frac{\partial H_x}{\partial z} \right) \delta E_x \, d\Omega \;=\; 0. \tag{3}$$

In this equation, the first term of the integrand contains second-order partial derivatives, and can be simplified by using Green's formula

$$\int_\Omega \triangle u \, v \, d\Omega \;=\; \int_\Gamma \frac{\partial u}{\partial n} v \, d\Gamma - \int_\Omega \nabla u \cdot \nabla v \, d\Omega.$$

Eq. (3) can then be written in the equivalent form

$$\begin{aligned} \frac{1}{i\omega\mu_0} \int_\Omega \nabla E_x \cdot \nabla \delta E_x \, d\Omega - \int_\Omega C E_x \, \delta E_x \, d\Omega - \int_\Omega A \frac{\partial H_x}{\partial y} \, \delta E_x \, d\Omega \\ + \int_\Omega B \frac{\partial H_x}{\partial z} \, \delta E_x \, d\Omega - \frac{1}{i\omega\mu_0} \int_\Gamma \frac{\partial E_x}{\partial n} \, \delta E_x \, d\Gamma = 0. \end{aligned} \tag{4}$$

Similarly, equation (2) is multiplied by an arbitrary variation of the magnetic component δH_x and integrated over the region Ω, and, subsequently, modified by using the following formula

$$\int_\Omega \nabla \cdot \mathbf{u} \, v \, d\Omega \;=\; \int_\Gamma \mathbf{u} \cdot \mathbf{n} \, v \, d\Gamma - \int_\Omega \mathbf{u} \cdot \nabla v \, d\Omega,$$

which eventually leads to the following integral equation

$$\begin{aligned} \int_\Omega \nabla \delta H_x \cdot (\underline{\underline{\tau}} \nabla H_x) \, d\Omega - \int_\Omega i\omega\mu_0 \, H_x \, \delta H_x \, d\Omega + \int_\Omega \mathbf{p} \cdot \nabla \delta H_x \, d\Omega \\ - \int_\Gamma \left(\underline{\underline{\tau}} \frac{\partial H_x}{\partial n} + \mathbf{p} \cdot \mathbf{n} \right) \delta H_x \, d\Gamma = 0, \end{aligned} \tag{5}$$

where $\mathbf{p} = -A E_x \mathbf{e_y} + B E_x \mathbf{e_z}$, $\mathbf{e_y}$ and $\mathbf{e_z}$ are the unit vectors along the $y-$ and $z-$axis, respectively.

The model area Ω is subdivided into rectangular elements. Within the FE approximation, we assume

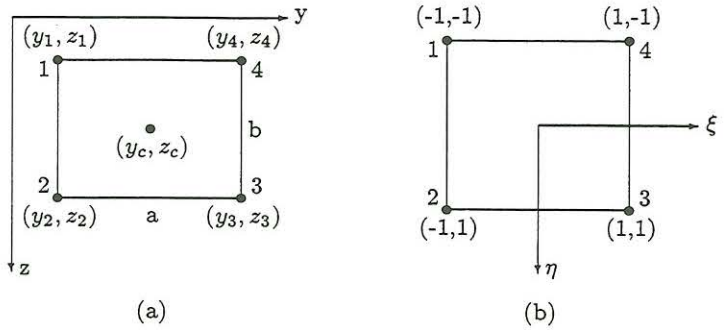

Fig. 2 Sub-element (a) and parent element (b).

that the electric field E_x and the magnetic field H_x are linear functions of y and z in each of the elements, and can be approximated by

$$E_x = \sum_{i=1}^{4} N_i E_{x_i}, \qquad H_x = \sum_{i=1}^{4} N_i H_{x_i}. \tag{6}$$

where E_{x_i} and H_{x_i} are the electric and magnetic fields at the corner point i, $i = 1, \cdots, 4$, of the sub-element (Fig. 2(a)), and N_i are linear shape functions defined as

$$N_i = \frac{1}{4}(1 + \xi_i \xi)(1 + \eta_i \eta), \quad i = 1, \cdots, 4, \tag{7}$$

where ξ_i and η_i are the coordinates of the corner point i, $i = 1, \cdots, 4$, of the parent element (Fig. 2(b)). The coordinate transformation between the parent element and a particular sub-element is

$$y = y_0 + \frac{a}{2}\xi, \quad z = z_0 + \frac{b}{2}\eta,$$

where y_0 and z_0 are the coordinates of the center of the sub-element, and a and b are the width and height of the rectangular element respectively.

The integrals in (4) and (5) are evaluated in the parent element by using equations (6) and (7). Finally, we get a system of $2n_d$ linear equations

$$\mathbf{KU} = 0, \tag{8}$$

where

$$\mathbf{K} = \begin{pmatrix} \mathbf{K_{11}} & \mathbf{K_{12}} \\ \mathbf{K_{21}} & \mathbf{K_{22}} \end{pmatrix}, \quad \mathbf{U} = \begin{pmatrix} \mathbf{E_x} \\ \mathbf{H_x} \end{pmatrix},$$

in which $\mathbf{K_{11}}$ and $\mathbf{K_{22}}$ are symmetric square matrices of the order n_d (n_d is the total number of nodal points in the entire model area Ω), and $\mathbf{K_{12}}$ and $\mathbf{K_{21}}$ are non-symmetric square matrices of the order n_d that, however, satisfy the symmetry relation $\mathbf{K_{12}} = \mathbf{K_{21}}^{\mathrm{T}}$. Hence, the $2n_d \times 2n_d$ matrix $\mathbf{K}$ is symmetric and sparsely occupied.

Substituting the boundary condition on the outer boundary into the equations (8), these equations can be solved for the field components E_x and H_x at the internal mesh nodes. The derived field components E_y, E_z, H_y and H_z are computed according to these forms:

$$\begin{aligned} H_y &= \frac{1}{i\omega\mu_0}\frac{\partial E_x}{\partial z}, \qquad H_z = -\frac{1}{i\omega\mu_0}\frac{\partial E_x}{\partial y}, \\ E_y &= \frac{\sigma_{yz}}{D}\frac{\partial H_x}{\partial y} + \frac{\sigma_{zz}}{D}\frac{\partial H_x}{\partial z} + BE_x, \\ E_z &= -\frac{\sigma_{yy}}{D}\frac{\partial H_x}{\partial y} - \frac{\sigma_{zy}}{D}\frac{\partial H_x}{\partial z} + AE_x. \end{aligned}$$

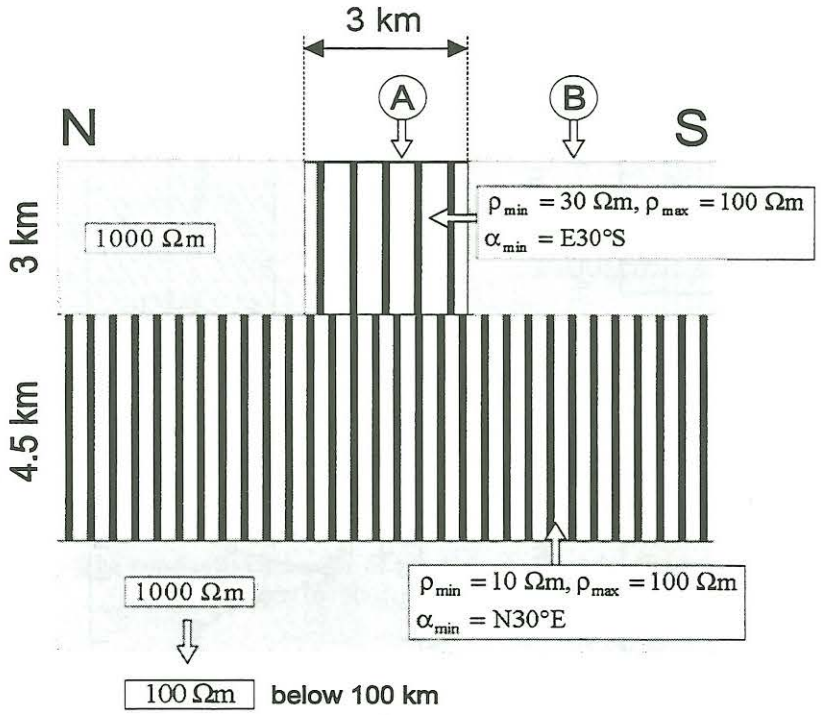

Fig. 3 Test model for comparison of FD and FE solutions: Outcropping anisotropic block underlain by an anisotropic layer.

The appropriate derivatives are evaluated numerically by the spline interpolation in our algorithm. The apparent resistivity and impedance phases are:

$$\rho_{ij} = \frac{1}{\omega\mu_0}|Z_{ij}|^2$$
$$\phi_{ij} = \tan^{-1}\frac{Im(Z_{ij})}{Re(Z_{ij})}, \quad i,j = x,y.$$

3 Numerical test

In order to test our theory and program, the computed FE results for a test model were compared with those obtained by the finite difference method (FD).

Figure 3 shows the test model presented by Pek & Verner (1997). A horizontally anisotropic layer underlies an outcropping horizontally anisotropic 2-D block. The anisotropy strikes of the two structures involved are perpendicular to one another, and unaligned with the structural strike of the 2-D model. The model was chosen in order to demonstrate serious distortions of the MT data caused by a complicated anisotropic situation. In Fig. 4, the computed FE results for the period of 30 s are compared with those of Pek & Verner (1997). The results show an excellent agreement.

4 Effects of the anisotropy

A 2-D anisotropic slab model is embedded into an isotropic homogeneous halfspace with $\rho_0 = 1000\Omega m$. The following basic forms of ansiotropy are distinguished:

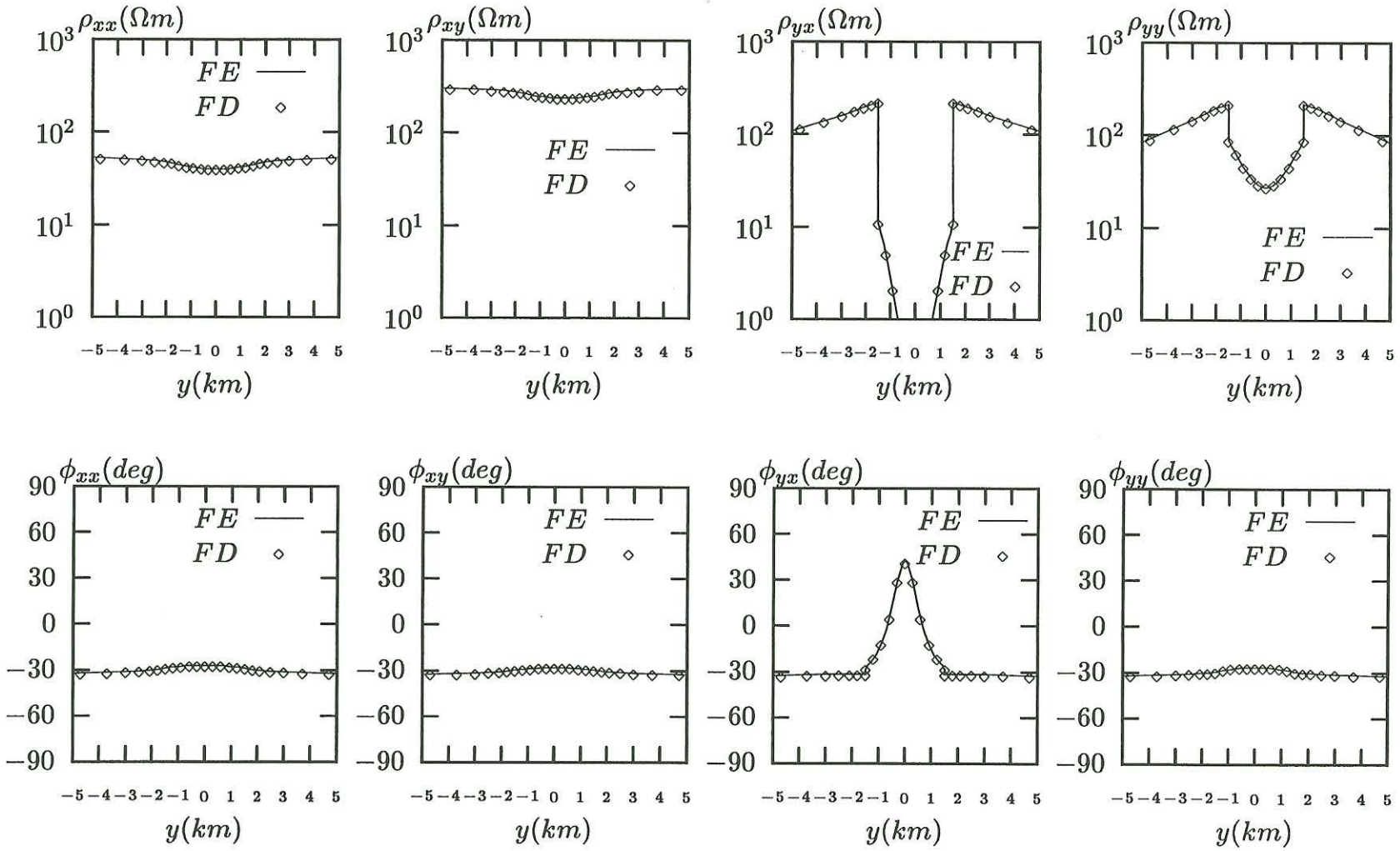

Fig. 4 Apparent resistivities (top) and phases (bottom) for the model in **Fig. 3.** Diamonds - results of the FD algorithm (Pek & Verner 1997); solid line - results of here presented FE algorithm.

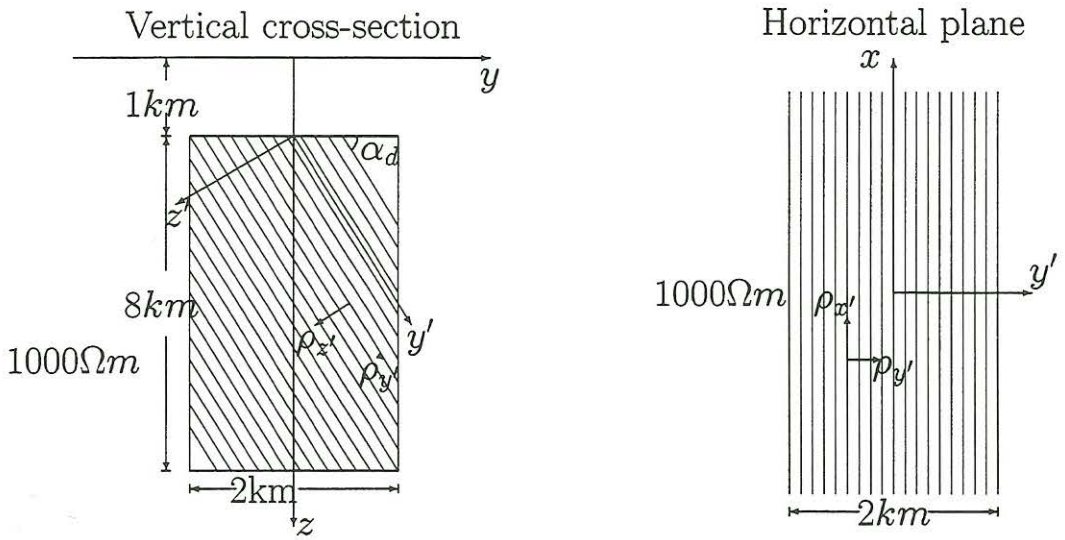

Fig. 5 A 2D slab with dipping anisotropy in an isotropic homogeneous halfspace with $\rho_0 = 1000\Omega m$. The conductivity tensor of the slab is givien by the principal resistivities $\rho_{x'}/\rho_{y'}/\rho_{z'} = 500/10/500\Omega m$ and the dipping angles α_d.

Dipping anisotropy (Fig. 5) One principal axis x' of the conductivity tensor is horizontal and parallel to the strike direction x, the remaining two principal axes y' and z' are in the vertical plane (y, z) with dipping angles α_d with respect to the y axis. The principal resistivities of the anisotropic inhomogeneity are $\rho_{x'}/\rho_{y'}/\rho_{z'} = 500/10/500$, in Ωm. Figure 6 shows the apparent resistivities for various dip angles α_d at the period of 10 s, when half space skindepth is $50km$. This figure indicates that:

1) the apparent resistivities ρ_{xy} are independent of the dip angle α_d, as the magnetotelluric field depends solely on $\rho_{xx} \equiv \rho_{x'}$ in this case and is not affected by the anisotropy;

2) the apparent resistivities ρ_{yx} are affected considerably by α_d. The ρ_{yx} curves are not symmetric with respect to the center of the model, the minimum of the curves is off-center and shifted to one side depending on the sign of the dip. This shift increases with increasing deviation of the dip from either the horizontal or vertial direction;

3) if $\alpha_d = 0$, ρ_{yx} corresponds to the apparent resistivity produced by a model with the resistivities 10 Ωm along y direction and 500 Ωm along the x and z directions. Similarly, if $\alpha_d = 90°$, ρ_{yx} corresponds to that produced by a model with vertical anisotropy, with the resistivities 500 Ωm along x and y directions and 10 Ωm along z direction.

Horizontal anisotropy (Fig. 7) One principal axis z' of the conductivity tensor is vertical, the remaining two principal axes x' and y' are in the horizontal plane (x, y) with strike angles α_s with respect to the x axis. The principal resistivities of the anisotropic inhomogeneity are $\rho_{x'}/\rho_{y'}/\rho_{z'} = 100/10/100$, in Ωm. According to a procedure proposed by Siemon (Siemon 1997), the magnitudes of the rotated off-diagonal impedance elements, $|Z_{x'y'}|$ and $|Z_{y'x'}|$, are plotted along the coordinate axes, rotated into the Swift principal direction, and the diagonal impedances, $|Z_{x'x'}|$ and $|Z_{y'y'}|$ attached to them as cross-bars. Figure 8 shows the magnetotelluric impedances in Siemon's representation along a surface profile for various strike angles α_s at a period of 10 s. From Fig. 8 we can conclude that

1) immediately above the anisotropic block, the minimum and maximum axes indicate the direction of high and low conductivity, respectively;

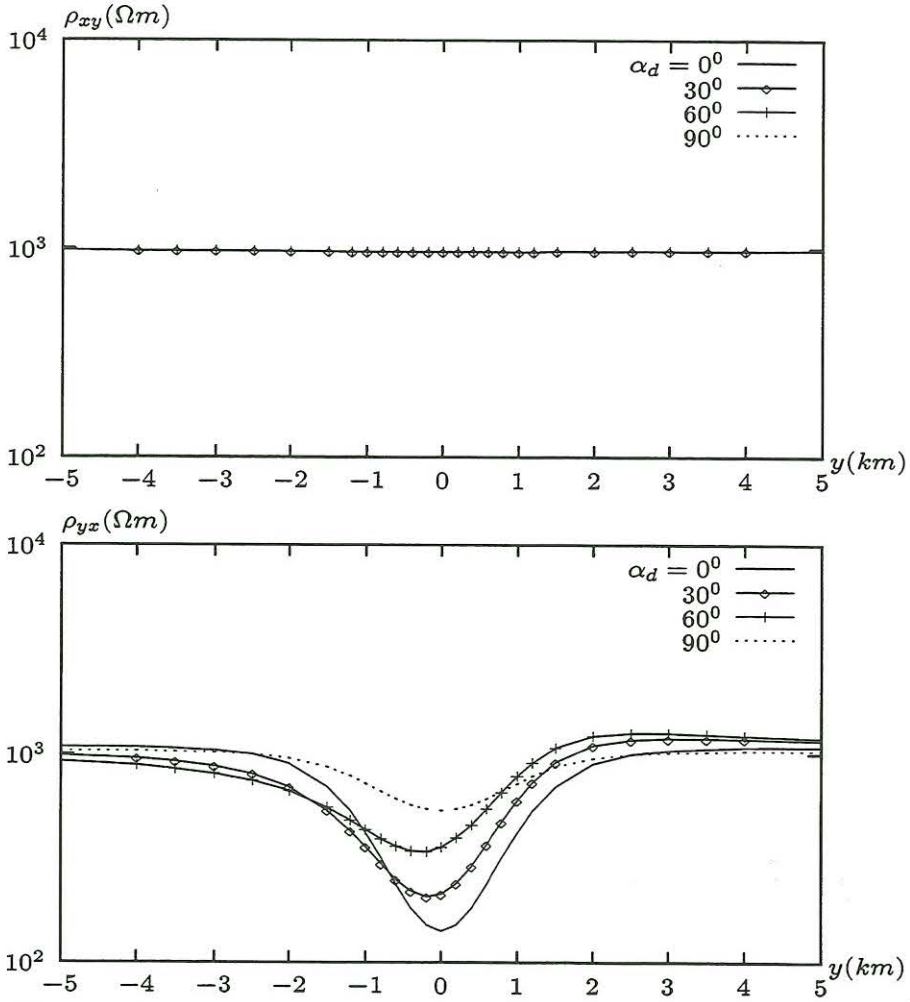

Fig. 6 Apparent resistivities for various dipping angles α_d at $T = 10s$ from **Fig. 5.**

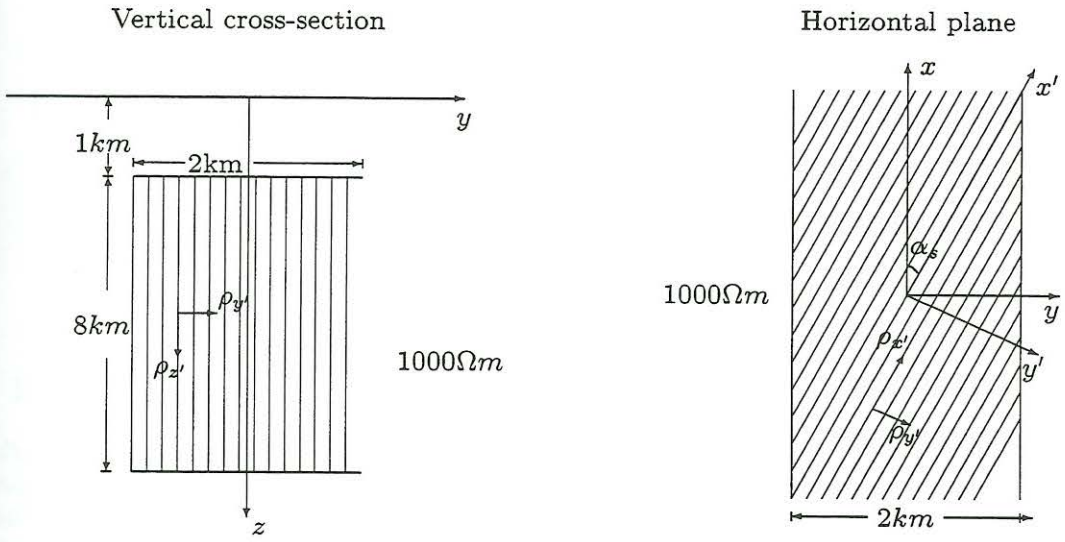

Fig. 7 A 2D slab with horizontal anisotropy in an isotropic homogeneous halfspace with $\rho_0 = 1000\Omega m$. The conductivity tensor of the slab is givien by the principal resistivities $\rho_{x'}/\rho_{y'}/\rho_{z'} = 500/10/500\Omega m$ and the anisotropic strikes α_s.

2) significant diagonal elements of the impedance tensor $|Z_{x'x'}|$ and $|Z_{y'y'}|$ exist except $\alpha_s = 0^0$ and 90^0, and become greater for greater deflections of the anisotopy strike α_s from the structural strike of the model;

3) far from the inhomogeneity, where the anomalous field fades out, the off-diagonal elements become equal and the diagonal elements disappear. When passing through the edge of the anisotropic block towards the homogeneous half-space, a certain reduction of the impedances take place within a transition zone where the above directional pattern can be severely distorted, especially if large anisotropies and shallow anomalous conductors are involved.

Vertical anisotropy The orientation of principal axes as before, but $\rho_{x'} = \rho_{y'}$, yielding different conductivity in vertical and any horizontal direction. Identical with special dipping anisotropy from above, if $\alpha_d = 90^0$.

5 conclusion

We have presented an algorithm for numerical modelling of magnetotelluric fields in generally anisotropic 2-D structures. There are the following special features of our numerical scheme:

1) the conductivity tensor of each anisotropic block is represented by a symmetric 3×3 matrix, thus general, horizontal, vertical and dipping anisotropies can be considerated;

2) the algorithm is based upon the finite element (FE) method which is better suited to sloping boundaries and topography;

3) assuming the air conductivity very small and positive, the air layer can be integrated into the conductive model. The equations for both modes can be approximated in the entire model area, which makes the approximation process much more simple;

4) the modified conjugated gradient technique is used to solve the equation system (8) which is complex symmetric. We found that a simple diagonal scaling (Jacobi Scaling) is a sufficient preconditioner;

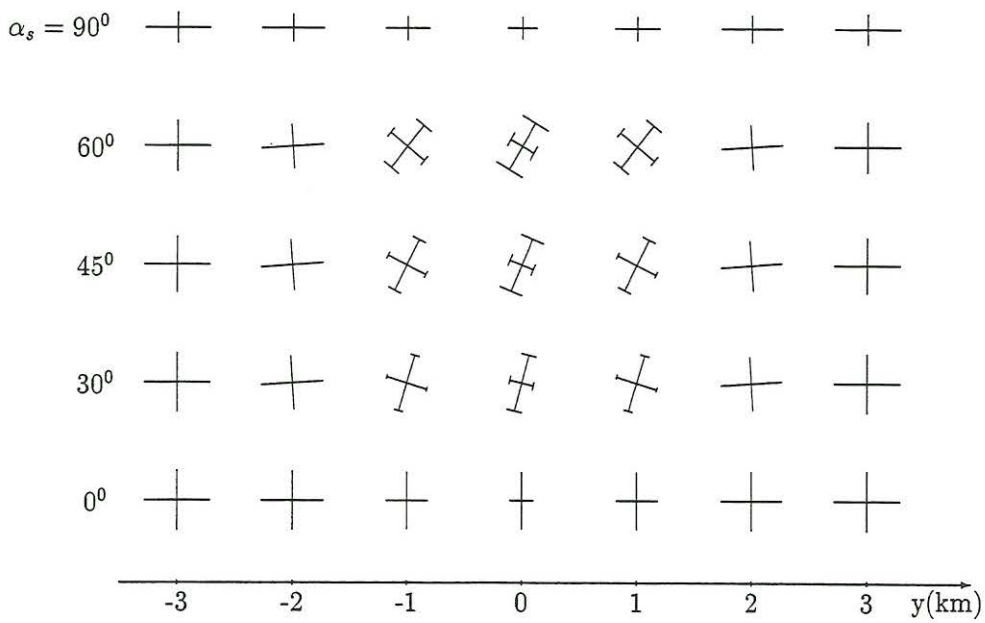

Fig. 8 MT principal axes for various strike angles α_s at $T = 10s$ from **Fig. 7.** Cross - absolutre values $Z_{x'y'}, Z_{y'x'}$; Crossbars - absolute values $Z_{x'x'}, Z_{y'y'}$; Rotated coordinates (x', y') according to Swift.

5) the spatial derivatives are computed numerically by the spline interpolation.

Acknowledgments I would like to express thanks to Dr. U. Schmucker and Dr. J. Pek for many stimulating discussions. Dr. J. Pek also provided the 1-D forward program for MT anisotropic structure and the FD results for the test model.

References

[1] Li,Y., 2000. *Numerische Modellierungen von elektromagnetischen Feldern in 2- and 3-dimenionalen anisotropen Leitfähigkeitsstrukturen der Erde nach der Methode der Finiten Elemente*, Ph.D. thesis, in Vorbereitung.

[2] Osella,A.M. and Martinelli,P., 1993. Magnetotelluric response of anisotropic 2-D structures, *Geophys. J. Int.*, **115**, 819-828.

[3] Pek,J. and Verner,T., 1997. Finite-difference modelling of magnetotelluric fields in two-dimensional anisotropic media, *Geophys. J. Int.*, **128**, 505-521.

[4] Reddy,I.K. and Rankin,D., 1975. Magnetotelluric response of laterally inhomogeneous and anisotropic media, *Geophysics*, **40**, 1035-1045.

[5] Schmucker,U., 1994. 2-D Modellrechnungen zur Induktion in inhomogenen dünnen Schichten über anisotropen geschichteten Halbräumen, in *Protokoll Koll. erdmagnetische Tiefenforschung, Höchst in Odenwald*, edited by Bahr,K. and Junge, A., 3-26.

[6] Schwarz, H. R., 1991. *Methode der finiten Elemente*, Teubner Verlag, Stuttgart .

[7] Siemon,B., 1997. An interpretation technique for superimposed induction anomalies, *Geophys. J. Int.*, **130**, 73-88.